Int. J. Heat Mass Transfer. Vol. 27, No. 9, pp. 1587–1594, 1984
Printed in Great Britain

0017-9310/84 $3.00 + 0.00

Reflux condensation in a two-phase closed thermosyphon

S. J. CHEN, J. G. REED and C. L. TIEN
Department of Mechanical Engineering, University of California, Berkeley, CA 94704, U.S.A.

(*Received* 16 *January* 1984)

Abstract—The reflux condensation flow phenomena in a two-phase closed thermosyphon are investigated experimentally and analytically by considering the countercurrent vapor–liquid flow occurring in this device. The analysis predicts that the liquid-film thickness is increased by vapor shear, resulting in a reduction of heat transfer compared to that calculated from Nusselt's solution. The experimental results indicate that Nusselt's solution for film condensation cannot interpret satisfactorily the observed trends and that inclusion of vapor shear effects alone does not rectify the discrepancy.

1. INTRODUCTION

THE TWO-phase closed thermosyphon used in this study is essentially a gravity-assisted wickless heat pipe, which is very efficient for the transport of thermal energy via phase change of the working fluid. In this work, reflux condensation in a two-phase closed thermosyphon is examined both analytically and experimentally. The term reflux condensation refers to the return of liquid condensate through condensation of rising vapor. Figure 1 illustrates schematically a two-phase closed thermosyphon. Vapor generated due to input of heat in the liquid reservoir at the bottom of the device rises up the tube and condenses on the cooled tube wall at the top of the device. The condensate then returns to the evaporator in the form of a falling liquid film driven solely by gravity. Because of the alignment of the device with respect to gravity, the condensate can be returned to the evaporator without the requirement of a capillary pressure head as needed in conventional heat pipes using porous wick structures [1, 2]. Since there is no wick material, the thermosyphon is simpler in construction, smaller in thermal resistance, and wider in its operating limits than the wicked heat pipe.

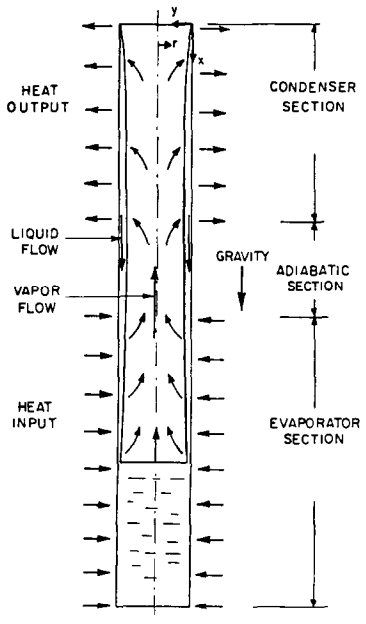

FIG. 1. A two-phase closed thermosyphon.

The operating characteristics of a two-phase closed thermosyphon have been investigated extensively in recent years [3–11]. There still exists, however, considerable uncertainty in the description of heat transfer characteristics. In particular, the existing works focus mostly on the overall system performance of the two-phase closed thermosyphon. Little information is available for the description of the local behaviors of the flows in both phases. The reason lies in the inherent complexity of the coupled transport phenomena.

The objective of the present work is to gain understanding of the heat transfer processes involved in reflux condensation of countercurrent liquid–vapor flows. It includes, specifically, an analytical investigation of the retardation of condensation by vapor shear and an experimental study of the local heat transfer coefficient of condensation.

2. REFLUX CONDENSATION WITH INTERFACIAL SHEAR

2.1. *Fundamental formulation*

In the following analysis, an annular flow is assumed in the condenser of the thermosyphon. Figure 1 shows the physical model. Since the liquid film is much smaller than the tube radius, the curvature effect can be neglected and the governing equations of boundary-layer type for a vertical plate can be applied to the condensate flow. In the current system, the heat capacity parameter, ζ $(= C_P \Delta T/h_{fg})$, and the acceleration parameter, ξ $(= \zeta/Pr)$, are both small. Thus, as in Nusselt's analysis [12], the fluid inertia and the energy convection can be neglected. The governing

NOMENCLATURE

A	surface area
B_L	parameter, $(4\xi L/\Delta)^{1/4}$
B_R	parameter, $\rho_v R/\rho\Delta B_L$
C_P	specific heat
F_τ	augmentation of interfacial shear by phase change
f_i	friction factor
g	gravitational acceleration
h	heat transfer coefficient
h_{fg}	latent heat of vaporization
k	thermal conductivity
L	condenser length
N_R	Nusselt number ratio, Nu/Nu_N
Nu	Nusselt number
P	dynamic pressure
Pr	Prandtl number
q	heat flux
R	radius
Re	film Reynolds number, Γ/μ
Re_v	vapor Reynolds number, $2\rho_v(u_v+u_i)R/\mu_v$
s	dimensionless axial coordinate, x/L
T	temperature
ΔT	temperature difference, T_v-T_w
u	x-component velocity
v	y-component velocity
x	axial coordinate
y	transverse coordinate.

Greek symbols

Γ	condensate mass flow rate per unit width
$\dot{\Gamma}$	condensation rate, $d\Gamma/dx$
γ	density ratio, ρ_v/ρ
Δ	characteristic length, $(v^2/[(1-\gamma)g])^{1/3}$
δ	film thickness
ζ	heat capacity parameter, $C_P\,\Delta T/h_{fg}$
η	similarity variable, $y/(4\xi\Delta^3 x)$
θ	dimensionless temperature
μ	viscosity
ν	kinematic viscosity
ξ	acceleration parameter, ζ/Pr
ρ	density
τ	shear stress
ϕ	augmentation factor of interfacial shear.

Subscripts

i	interface
v	vapor
w	wall.

Superscript

*	dimensionless quantity.

equations become

$$0=\mu\frac{\partial^2 u}{\partial y^2}-\frac{\partial P}{\partial x}+(\rho-\rho_v)g \tag{1}$$

$$0=\frac{\partial^2 T}{\partial y^2} \tag{2}$$

where P is the dynamic pressure of vapor. The associated boundary conditions are, at $y=0$:

$$u=v=0,\quad T=T_w \tag{3}$$

and at $y=\delta$:

$$\mu\frac{\partial u}{\partial y}=-\tau_i,\quad T=T_v \tag{4}$$

$$k\frac{\partial T}{\partial y}=\dot{\Gamma}h_{fg} \tag{5}$$

where the minus sign is introduced in accordance with the notations in Fig. 1 indicating a retardation of liquid flow, and

$$\dot{\Gamma}=\frac{d\Gamma}{dx}=\frac{d}{dx}\int_0^\delta \rho u\,dy.$$

Difficulties may arise in calculating the pressure drop unless the flow field in the evaporator is fully known. Fortunately, the pressure variation is usually small compared to the viscous forces acting on the liquid, although it is the pumping force for the vapor flow. To assess the pressure drop, a uniform one-dimensional (1-D) vapor flow at saturation temperature, T_v, is assumed. From mass conservation at each cross section, the velocity of vapor is given as

$$u_v=\frac{2\Gamma}{\rho_v R}$$

and the force balance for both phases yields

$$R\frac{dP}{dx}=-2\tau_w+2(\rho-\rho_v)g\delta-2\frac{d}{dx}\left(\frac{2\Gamma^2}{\rho_v R}\right) \tag{6}$$

where the liquid inertia is neglected and τ_w is the wall shear.

The motion of liquid, on the other hand, is governed by the driving force due to gravitation and the retarding force from the interfacial shear. At some particular vapor flow rate, the velocity at the interface vanishes. The interfacial shear and the gravitational force are of equal significance at this point. For vapor flow rates above this point, flow reversal occurs. Eventually, the interfacial shear becomes dominant and the system reaches the total flooding limit, i.e. the liquid flow is totally retarded. Regardless of the dominant forces, the pressure term in the momentum equation of the liquid is negligible as is seen from equation (6) by order of magnitude analysis.

Letting L be the condenser length and introducing the following variables

$$\gamma=\rho_v/\rho,\quad \Delta=[v^2/(1-\gamma)g]^{1/3},\quad s=x/L$$

$$\eta=y/(4\xi\Delta^3 x)^{1/4},\quad \delta^*=\delta/(4\xi\Delta^3 x)^{1/4}$$

$$u^*=u\Big/\left(\frac{4v^2\xi x}{\Delta^3}\right)^{1/2},\quad u_v^*=u_v\Big/\left(\frac{4v^2\xi x}{\Delta^3}\right)^{1/2}$$

$$\Gamma^* = \int_0^{\delta^*} u^* \, d\eta$$

$$\tau_i^* = \tau_i/(4\rho^4 g^4 \xi x \Delta^3)^{1/4}$$

$$\theta = (T - T_w)/(T_v - T_w)$$

equations (1)–(4) can be nondimensionalized and solved to give

$$u^* = (\delta^* - \tau_i^*)\eta - \eta^2/2 \tag{7}$$

$$\theta = \eta/\delta^*. \tag{8}$$

The following expressions can then be obtained

$$\Gamma^* = \delta^{*3}/3 - \delta^{*2}\tau_i^*/2 \tag{9}$$

$$u_i^* = \delta^{*2}/2 - \tau_i^*\delta^* \tag{10}$$

$$\tau_w^* = \delta^* - \tau_i^* \tag{11}$$

where $\tau_w^* = \partial u^*/\partial\eta|_{\eta=0}$. The dimensionless form of the condensation rate in equation (5) follows as

$$3\Gamma^* + 4s\frac{d\Gamma^*}{ds} = \frac{1}{\delta^*}. \tag{12}$$

Upon substitution of equation (9) into equation (12) there results

$$\frac{d\delta^*}{ds} = \frac{1 - \delta^{*4} + 1.5\delta^{*3}\tau_i^*}{4s\delta^{*2}(\delta^* - \tau_i^*)}. \tag{13}$$

Note that in the limiting case of $\tau_i^* = 0$, similarity exists and the problem reduces to Nusselt's analysis which gives $\delta^* = 1$.

The significance of interfacial shear can now be assessed. The dimensionless interfacial shear at the onset of flow reversal, occurring at the location where $u_i^* = 0$, is $\tau_i^* = \delta^*/2$, which indicates that the interfacial shear is comparable to the gravity force. At higher values of interfacial shear, the liquid flow may vanish. By letting $\Gamma^* = 0$, this point can be seen to occur when $\tau_i^* = 2\delta^*/3$. Further increase of vapor flow will totally retard the liquid flow. The total flooding point can be determined as the point where $\tau_w^* = 0$, which means that the velocity at the wall is maximum. Thus, at the total flooding point, $\tau_i^* = \delta^*$. It should be noted that the conclusion drawn above may not be strictly accurate since finite-amplitude waves are usually observed near the flooding point [13].

Rather than solving the vapor flow under conditions of reflux condensation, the interfacial shear can be specified using the Lockhart–Martinelli correlation [12] or the Fanning friction coefficient, f_i [14, 15]. In this work, the interfacial shear is evaluated as for fully developed pipe flow of the vapor with suction. To account for the augmentation of interfacial shear due to the momentum exchange of phase change, the following modification proposed by Blangetti and Nanshaki [16] is used

$$\tau_i = 0.5 f_i \frac{\phi}{e^\phi - 1}(u_v + u_i)^2 \tag{14}$$

where u_v is positive for upward flowing vapor and

$$\phi = -|\dot{\Gamma}|/(0.5 f_i \rho_v |u_v + u_i|). \tag{15}$$

The pure Fanning friction factor, f_i, is given, for pipe flow with no suction, by the following expressions [14]

$$f_i = 16/Re_v, \qquad Re_v < 200$$

$$f_i = Re_v^{0.33}/1525, \qquad 2000 < Re_v < 4000$$

$$f_i = 0.079 Re_v^{-0.25}, \qquad 4000 < Re_v < 30\,000$$

$$f_i = 0.046 Re_v^{-0.2}, \qquad 30\,000 < Re_v < 10^6.$$

Here, to be consistent, the vapor Reynolds number is defined in terms of the mean vapor velocity, u_v, and the interface velocity, u_i, as

$$Re_v = \frac{2\rho_v(u_v + u_i)R}{\mu_v} = \frac{4\Gamma}{\mu_v} + \frac{2\rho_v u_i R}{\mu_v}. \tag{16}$$

Using the above dimensionless variables, we have

$$Re_v = B_L^3(\mu/\mu_v)(4s^{3/4}\Gamma^* + 2B_R s^{1/2}u_i^*) \tag{17}$$

$$u_v^* = 2s^{1/4}\Gamma^*/B_R \tag{18}$$

$$\phi = -(R/L)/[2B_R s^{3/4}\delta^* f_i(u_v^* + u_i^*)] \tag{19}$$

and

$$\tau_i^* = 0.5 B_L^3\left(\frac{\rho_v}{\rho}\right) f_i s^{3/4}(u_v^* + u_i^*)\frac{\phi}{e^\phi - 1} \tag{20}$$

where equation (5) has been used to obtain equation (19) and

$$B_L = (4\xi L/\Delta)^{1/4}, \quad B_R = \rho_v R/(\rho \Delta B_L).$$

2.2. *Computational method*

A finite-difference scheme is adopted to solve the problem formulated above. Since the computation starts from the top of the thermosyphon, the dimensionless interfacial shear there has to be sought first. As s approaches zero, it can be shown that

$$f_i s^{3/4} \to 0, \quad \phi \to -\infty$$

and

$$f_i s^{3/4}\frac{\phi}{e^\phi - 1} \to \frac{R}{2LB_R\delta^* u_i^*}.$$

Therefore, at $s = 0$

$$\tau_i^* = \xi u_i^*/\delta^*.$$

Since ξ is small, equation (13) states that δ^* is very close to unity in the region near the top end of the condenser.

The computation proceeds by assuming an initial value of τ_i^* at each node. The value of δ^* is then found by equation (13). Equations (9), (10) and (18) are solved for Γ^*, u_i^* and u_v^*, respectively. A new distribution of τ_i^* is obtained by using equation (20). This procedure is repeated until the required convergence criterion is satisfied.

2.3. *Results and discussion*

In the following, numerical results for laminar film condensation including the effect of interfacial shear are

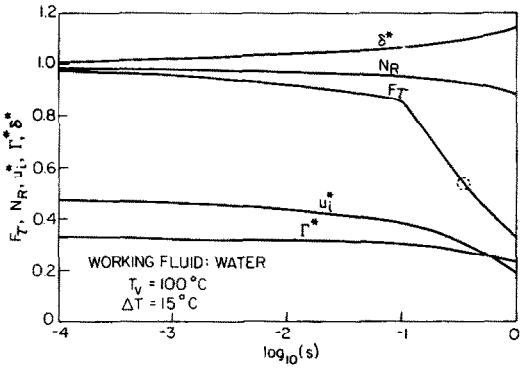

FIG. 2. Interfacial shear effect on reflux condensation for water at $T_v = 100°C$ and $\Delta T = 15°C$.

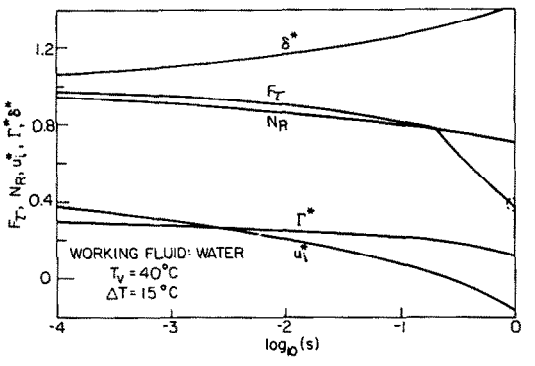

FIG. 3. Interfacial shear effect on reflux condensation for water at $T_v = 40°C$ and $\Delta T = 15°C$.

presented. All the cases reported are calculated for $L = 1$ m. Figure 2 shows the behavior of the film for water at $T_v = 100°C$ and $\Delta T = 15°C$. The distributions of film thickness, interface velocity and flow rate downward along the condenser are displayed. Also shown in the figure are $N_R = Nu/Nu_N$, the ratio of Nusselt number to that predicted by Nusselt's solution, and F_τ, the augmentation of interfacial shear due to phase change, defined by

$$F_\tau = 1 - \frac{\tau_{ad}^*}{\tau_i^*} = 1 - \frac{e^\phi - 1}{\phi}$$

where τ_{ad}^* is the interfacial shear calculated at the same vapor Reynolds number as if the wall were adiabatic. As mentioned before, near the top end of the condenser the effect of interfacial shear is small. Thus, if one extends all curves toward $s = 0$, they converge to Nusselt's solution.

It is seen that the effect of interfacial shear is to cause the liquid film to become thicker, the interface velocity to be slower and the flow rate of liquid to be lower than in cases where shear effects are absent. Therefore, the ratio of the heat transfer coefficient, N_R, decreases with s as a result of an increase in film thickness. The distribution of F_τ shows that at small s, the interfacial shear is mainly due to phase change and its effect on condensation is secondary. When the flow rate of vapor becomes so high as to be in the transition region from laminar into turbulent flow, as indicated by the sharp change of slope in the F_τ-curve, the decrease in heat transfer by vapor shear becomes appreciable. Further downstream, the vapor flow becomes fully turbulent and a second slope change in the F_τ-curve can be observed at the location marked by the dotted circle. While the augmentation of interfacial shear due to phase change is less significant in this region, the heat transfer coefficient continues to drop.

When vapor shear is appreciable, flow reversal may occur. As shown in Fig. 3 for water at $T_v = 40°C$ and $\Delta T = 15°C$, the interface velocity is negative over most of the condenser, indicating that some of the liquid flow is reversed across the condensate layer since the net mass flow rate is still positive. The decrease in heat transfer coefficient for this case is more pronounced than in the aforementioned case. Note that the difference in the film behaviors between Figs. 2 and 3 is caused by the different operating temperatures which can affect the thermophysical properties of the working fluid.

Since the properties of vapor are strongly dependent on temperature, it is expected that the effects of vapor shear on condensation will be different at other operating temperatures. Figures 4 and 5 exhibit heat transfer coefficients including the effect of vapor shear for various operating temperatures using water and methanol as working fluids. It is seen that at high operating temperatures, the effect of vapor shear on condensation is small. However, it becomes relatively important at low operating temperatures, especially for water. Since the values of the temperature difference, ΔT, are the same, the differences result from the variations of properties of vapor and liquid with temperature. Along the saturation curves, the density and viscosity of vapor increase with temperature while, for the liquid, these two properties decrease slightly with temperature. At high operating temperatures, the net effect of property variations is to have lower vapor velocity, higher vapor Reynolds number and smaller vapor shear effect as revealed by equations (17), (18) and (20), respectively.

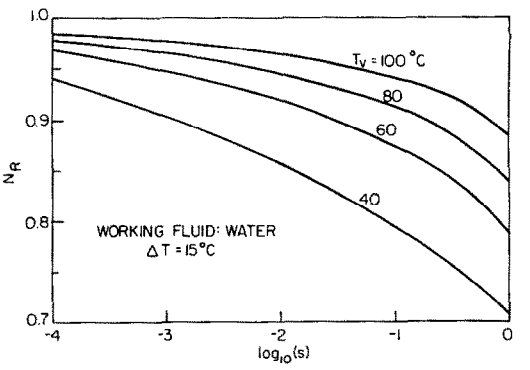

FIG. 4. Reduction in Nusselt number by vapor shear during reflux condensation of water at $\Delta T = 15°C$ and different operating temperatures, T_v.

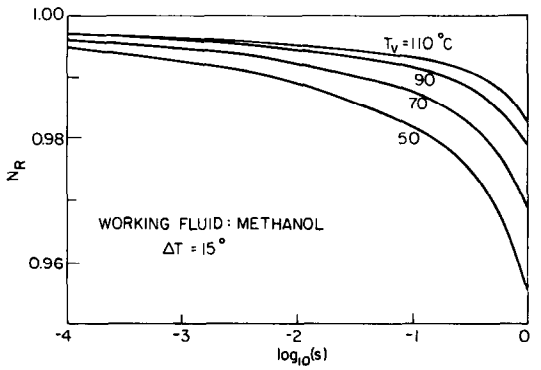

FIG. 5. Reduction in Nusselt number by vapor shear during reflux condensation of methanol at $\Delta T = 15°C$ and different operating temperatures, T_v.

It is noted that the effect of interfacial shear is more important in the water cases than in the methanol cases. This is because the ratio of liquid density to vapor density is larger for water, and the difference in the averaged velocities of both phases becomes relatively significant. Hence, the interfacial shear in the water cases modifies the liquid flow relatively more.

The effect of vapor shear can be expected to be more pronounced at larger flow rates of both phases. As ΔT is increased, the decrease in the heat transfer coefficient by vapor shear becomes larger. This can be easily seen since higher values of ΔT mean larger mass flow rates (ξ) and thus signify greater interfacial shear.

3. EXPERIMENTAL INVESTIGATION

3.1. *Apparatus*

A schematic diagram of the test apparatus is shown in Fig. 6. The system is composed of three sub-systems: the test section, the cooling water circulation system and the power supply. The test section is basically a two-phase closed thermosyphon, with a 14.2 mm I.D. As shown in Fig. 6, it is divided into three parts: evaporator, adiabatic section, and condenser. The total section length is 2.2 m. The evaporator section, which is an inconel tube with a wall thickness of 1.016 mm, is electrically heated by a DC power supply. Glass-wrapped chromel–alumel thermocouples are spot-welded on the outside surface of the inconel tube at six locations along its length. In the adiabatic section and the condenser section, the tubes are made of 19.05 mm O.D. stainless steel tubing. The local heat fluxes and temperatures in the condenser and adiabatic section are measured by Rdf Micro-Foil heat flow sensors (Model No. 20455-2) which have copper–constantan thermocouples built in. Five such sensor–thermocouple pairs are attached to the outside surface of the condenser and one pair to the adiabatic section by a special glue with high thermal conductivity. Each sensor is 27.94 mm in length and 12.7 mm in width. The sensor foil thickness is 0.127 mm. The maximum operating temperature is 260°C. An additional copper–constantan thermocouple is inserted into the tube through the upper end cap to measure the vapor temperature. The tip of it is exposed while the remainder is covered by a stainless steel sheath of 1.56 mm

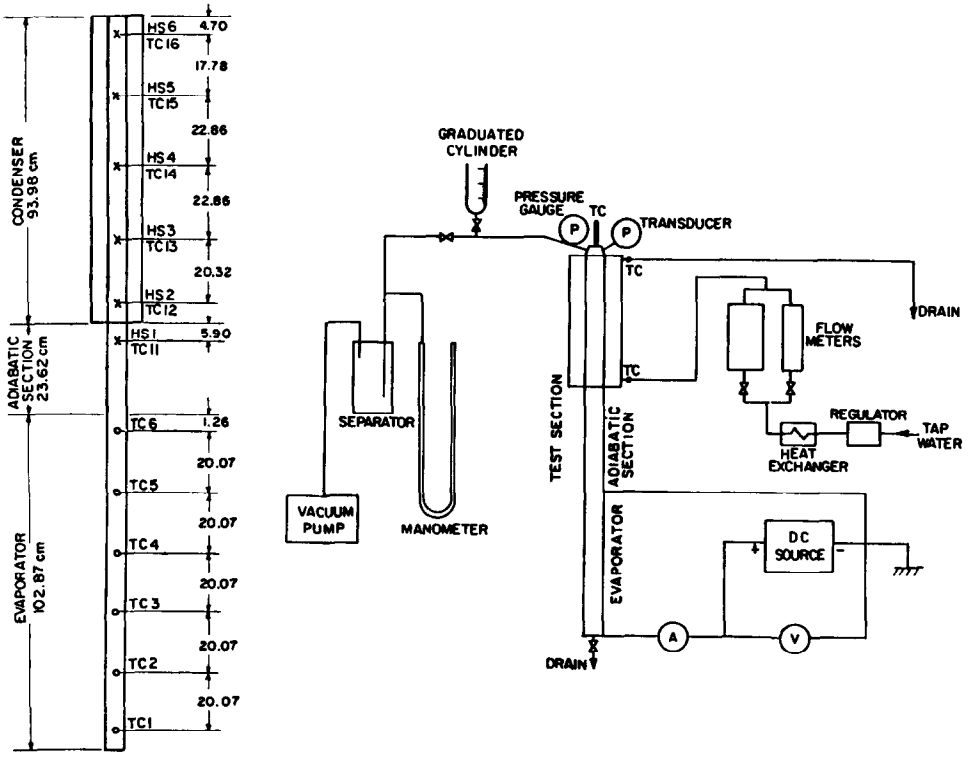

FIG. 6. Schematic diagram of experimental apparatus (HS, heat flow sensor; TC, thermocouple).

O.D. A strain gauge-type pressure transducer is mounted on the condenser end cap to measure the system pressure, i.e. the vapor pressure. In addition, the system pressure is also monitored by a bourdon-type gauge. The test section is insulated to minimize the heat loss. Cooling is provided by house water supply. A regulator is used to assure a constant coolant flow rate. A small heat exchanger is used to control the inlet cooling-water temperature, which in turn affects the system pressure.

Before operation, the test tube is thoroughly cleaned and vacuum dried. A known amount of working fluid is then charged into the tube. Heating is applied by passing current directly through the inconel evaporator. The cooling water is let into the jacket via the regulator and the flow meter. After the system reaches steady state, the temperatures, heat fluxes, heat input and flow rate are recorded.

3.2. *Data reduction*

The local heat transfer coefficient, h, at each location of the heat flow sensor indicated in Fig. 6 can be calculated directly from the measure of local heat flux, q, and average wall temperature, T_w

$$h = q/(T_v - T_w).$$

Here, the vapor temperature has been assumed uniform in the condenser. Also attainable from the experiments is the mass flow rate of the condensate per unit width, Γ. Using the fact that the top end of the thermosyphon is closed, the mass conservation requires that the mass flow rates of both phases be the same. Hence, a simple energy balance gives

$$\Gamma(x_i) = \sum_{n=1}^{i} \frac{A_n q_n}{h_{fg}}.$$

In this equation, q_n is the heat flux measured by sensor n, x_i is the sensor location, and A_n is the portion of the condenser area over which that heat flux is assumed to apply. It is assumed that the heat flux measured by each sensor applies to the region delimited by the midpoints of the segments to the two adjacent sensors. If the sensor is adjacent to a boundary, A_n extends to the boundary. In view of the measured heat flux distributions, this assumption appears reasonable over most of the condenser except in the region near the closed end.

3.3. *Experimental results*

The entire body of data collected from the steady-state operation of the device is shown in Fig. 7. This plot represents a variety of operating temperatures and pressures for both methanol and water. For comparison, the theoretical Nusselt's solution and its improvement taking into account the effect of interfacial shear are plotted along with the experimental data. The curve corrected for vapor shear effect is for the case of maximum vapor shear among the test conditions.

As can be seen in the figure, the data are quite scattered about Nusselt's solution. However, it appears

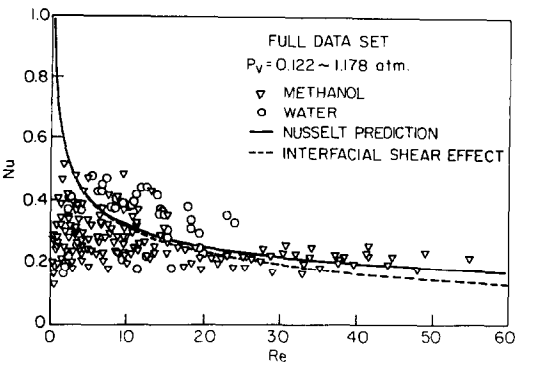

FIG. 7. Experimental data of reflux condensation at a wide range of system pressures.

that at relatively high Reynolds numbers ($10 < Re < 30$), the condensation heat transfer is higher than that predicted by Nusselt theory. The observed increase of heat transfer coefficients may be attributed partly to the waviness of the film which will be discussed in subsequent work, and partly to the liquid carry-over from the evaporator. At higher Reynolds numbers, this increase is offset by the interfacial shear due to the turbulent vapor flow. On the other hand, the data at low Reynolds numbers fall below the predicted results. It is believed that this occurs because of certain aspects of the condensation problem which are particular to a closed device such as that used in this study. It is noted that most of the low Reynolds number data represent the behavior at the top of the thermosyphon.

There are several effects which may account for the low values of the heat transfer coefficient occurring at the top of the device. First, any non-condensable gases present in the system will move upward with the bulk vapor flow and accumulate at the top of the condenser. As a result, the gas-occupied portion of the condenser is nearly shut off and the active condenser area is reduced. Moreover, the gas front will also tend to spread along the liquid–vapor interface [17] and thus will present a diffusive resistance to the vapor migrating to the interface which further reduces condensation.

A second factor which may contribute to the low heat transfer readings at the top of the device is that the end cap is not perfectly insulated. A thick liquid film may be established near the top end due to the Marangoni effect [18] which accounts for the variation of surface tension over the film surface caused by axial temperature drop. The thermal end effects discussed here are, however, not believed to be responsible for the trend in the data because application of an external guard heater to the end cap results in little change in the device performance.

Another possible explanation is that no liquid film exists at the top of the device. This is particularly true for water at low pressures. During certain test runs, the steady-state heat transfer in the upper portion of the device was nearly zero. In addition, the wall temperatures were also observed to be close to that of the heat sink (cooling water). Since heat transfer was

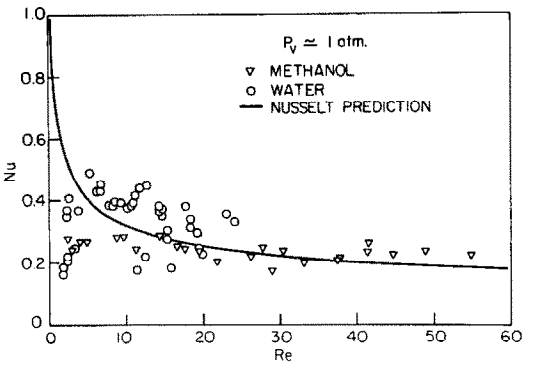

FIG. 8. Experimental data of reflux condensation at $P \simeq 1$ atm.

very small in this portion, the wall and vapor temperatures were nearly equal. This indicated that little condensation was occurring in this region of the device and the liquid film was absent. At low pressures, the vapor flow rate generated by the input heat is probably not high enough to reach the upper portion of the condenser. This is because the upward flowing vapor will eventually be totally consumed by condensation. If the pipe is long enough, the vapor flow generated at low pressures may be unable to adjust itself to have film condensation start from the top end of the thermosyphon. Some droplets may be present on the tube wall in these locations, but the condensation rate will be very small.

The effects at the top of the device as mentioned above should be much less evident if only data for relatively high system pressures are considered and if the data from the flux sensor closest to the end cap are omitted. As the system pressure is increased, less leakage of non-condensable gas into the system would be expected. Therefore, this subset of data should not show the low values of heat transfer coefficient at low Reynolds numbers which are evident in the full data set. Figure 8 displays this subset of data. All the data are for system pressures near 1 atm which is the maximum pressure range among the test conditions. As expected, the anomalous behavior seen in Fig. 7 is much less evident in Fig. 8, although a few points substantially below the theoretical curve are still observed.

4. CONCLUSIONS

A theoretical analysis of the influence of vapor drag on condensation in countercurrent vapor–liquid flow was included in the present work. The vapor drag on the liquid surface was assessed by introducing modified Fanning friction factors which incorporate the augmentation of interfacial shear through phase change and the velocity difference between liquid and vapor phases. The numerical results indicate that the interfacial shear in the laminar vapor flow regime is mainly due to phase change and here the decrease in heat transfer by vapor shear is small. When the vapor flow becomes turbulent, the importance of the augmentation of interfacial shear by phase change rapidly becomes small, although it cannot be ignored under the conditions in the present study. However, the decrease in heat transfer by vapor shear in this regime becomes appreciable. For the cases under consideration, the reduction of heat transfer by vapor drag in the water case is much more significant than that in the methanol cases.

A series of experiments was performed to examine the film behaviors during reflux condensation. Emphasis was placed on the measurement of local heat transfer rates. The whole set of experimental results was reduced in dimensionless form and compared to Nusselt's solution. It was found that at low Reynolds numbers the data fall below Nusselt prediction, but at high Reynolds numbers, the condensation heat transfer coefficients are underpredicted. Several possible factors were discussed to explain such trends. The experimental results indicate that Nusselt's solution cannot satisfactorily explain the film flow and that improvements of this simple analysis are needed.

Acknowledgements—The authors express their appreciation to the Electric Power Research Institute for the support of this research under Contract EPRI RP 1160-3. Discussions and comments from Dr Jean Pierre Sursock of EPRI were very helpful to the conduct of this work.

REFERENCES

1. C. L. Tien, Heat pipes, in *Handbook of Heat Transfer*, Chap. 19. McGraw-Hill, New York (1984).
2. P. Dunn and D. A. Reay, *Heat Pipes* (3rd edn.). Pergamon Press, New York (1982).
3. Y. Lee and U. Mital, A two-phase closed thermosyphon, *Int. J. Heat Mass Transfer* **15**, 1695–1707 (1972).
4. M. Shiraishi, K. Kikuchi and T. Yamanishi, Investigation of heat transfer characteristics of a two-phase closed thermosyphon, in *Advances in Heat Pipe Technology* (edited by D. A. Reay), pp. 95–104. Pergamon Press, New York (1981).
5. W. K. Ho and C. L. Tien, Reflux condensation characteristics of a two-phase closed thermosyphon, in *Advances in Heat Pipe Technology* (edited by D. A. Reay), pp. 451–458. Pergamon Press, New York (1981).
6. F. E. Andros and L. W. Florchuetz, The two-phase closed thermosyphon: an experimental study with flow visualization, in *Two-phase Transport and Reactor Safety* (edited by T. N. Veziroglu), pp. 1231–1267. Hemisphere, Washington, DC (1978).
7. H. Ngueyen-Chi and G. Groll, Entrainment or flooding limit in a closed two-phase thermosyphon, in *Advances in Heat Pipe Technology* (edited by D. A. Reay), pp. 147–162. Pergamon Press, New York (1981).
8. C. Casarosa, E. Latrofa and A. Shelginski, The geyser effect in a two-phase thermosyphon, *Int. J. Heat Mass Transfer* **26**, 933–941 (1983).
9. H. Imura, K. Sasaguchi, H. Kozai and S. Numata, Critical heat flux in a closed two-phase thermosyphon, *Int. J. Heat Mass Transfer* **26**, 1181–1188 (1983).
10. K. Negishi and T. Sawada, Heat transfer performance of an inclined two-phase closed thermosyphon, *Int. J. Heat Mass Transfer* **26**, 1207–1213 (1983).
11. T. Fukano, S. J. Chen and C. L. Tien, Operating limits of the two-phase closed thermosyphon, *ASME-JSME Thermal Engineering Joint Conference Proceedings*, Hawaii, Vol. 1, pp. 95–101 (1983).

12. M. M. Rohsenow, Condensation, in *Handbook of Heat Transfer* (edited by M. M. Rohsenow and J. P. Hartnett). McGraw-Hill, New York (1973).
13. C. L. Tien, C. P. Liu and K. S. Chung, A review of vertical two-phase countercurrent flooding, in *Heat and Mass Transfer in Metallurgical Systems* (edited by D. S. Spalding), pp. 609–614. Hemisphere, Washington, DC (1979).
14. R. A. Seban and J. A. Hodgson, Laminar film condensation in a tube with upward vapor flow, *Int. J. Heat Mass Transfer* **25,** 1291–1299 (1982).
15. B. K-H. Sun, M. Toren and S. Oh, Reflux condensation in a vertical channel flow, *Proc. 2nd Int. Topical Meeting on Nuclear Reactor Thermal Hydraulics*, Santa Barbara, California (1983).
16. F. Blangetti and M. K. Nanshaki, Influence of mass transfer on the momentum transfer in condensation and evaporation phenomena, *Int. J. Heat Mass Transfer* **23,** 1694–1695 (1980).
17. K. Hijikata, S. J. Chen and C. L. Tien, Non-condensable gas effect on condensation in a two-phase closed thermosyphon, *Int. J. Heat Mass Transfer* **27,** 1319–1325 (1984).
18. G. F. Hewitt and N. S. Hall-Taylor, *Annular Two-phase Flow*. Pergamon Press, Oxford (1970).

CONDENSATION DE REFLUX DANS UN THERMOSYPHON DIPHASIQUE FERME

Résumé—Le phénomène d'écoulement de condensation avec reflux dans un thermosyphon diphasique fermé est étudié expérimentalement et analytiquement en considérant l'écoulement à contrecourant vapeur–liquide fonctionnant dans cette condition. L'analyse prédit que l'épaisseur liquide-film est augmentée par le cisaillement de la vapeur, ce qui conduit à une réduction du transfert thermique comparé à celui calculé par la solution de Nusselt. Les résultats expérimentaux montrent que la solution de Nusselt pour la condensation en film ne peut interpréter correctement les tendances observées et que l'inclusion des seuls effets du cisaillement de la vapeur ne peut rectifier le désaccord.

RÜCKSTROM-KONDENSATION IN EINEM GESCHLOSSENEN ZWEI-PHASEN-THERMOSYPHON

Zusammenfassung—Die Strömungsvorgänge bei der Rückstrom-Kondensation in einem geschlossenen Zwei-Phasen-Thermosyphon wurden experimentell und analytisch untersucht. Hierzu wurde die gegenläufige Dampf–Flüssigkeits–Strömung, die in einer derartigen Apparatur auftritt, betrachtet. Aus den theoretischen Überlegungen folgt, daß die Kondensatfilmdicke durch die vom Dampfstrom aufgeprägte Schubspannung zunimmt und infolge dessen der Wärmeübergang im Vergleich zur Nusselt'schen Theorie schlechter wird. Die experimentellen Ergebnisse zeigen, daß die Nusselt'sche Theorie der Film-Kondensation nicht in der Lage ist, die beobachteten Resultate zu erklären und daß die Abweichungen nicht allein durch den Einfluß der Dampfschubspannung zu begründen sind.

КОНДЕНСАЦИЯ В ДВУХФАЗНОМ ЗАМКНУТОМ ТЕРМОСИФОНЕ

Аннотация—Явления течения с конденсацией в двухфазном замкнутом термосифоне исследуются экспериментально и аналитически на основе рассмотрения противоточного течения пара и жидкости в этом устройстве. Анализ показывает, что толщина жидкой пленки увеличивается за счет касательного напряжения в паре, что приводит к снижению величины передаваемого теплового потока по сравнению со значением, полученным из решения Нуссельта. Экспериментальные результаты свидетельствуют о том, что решением Нуссельта нельзя удовлетворительно описывать пленочную конденсацию и что учет только эффектов касательного напряжения в паре не позволяет получить точных результатов.